SINTEF
PROCEEDINGS
2

Proceedings of the 12th International Conference on Computational Fluid Dynamics in the Oil & Gas, Metallurgical and Process Industries

Progress in Applied CFD – CFD2017

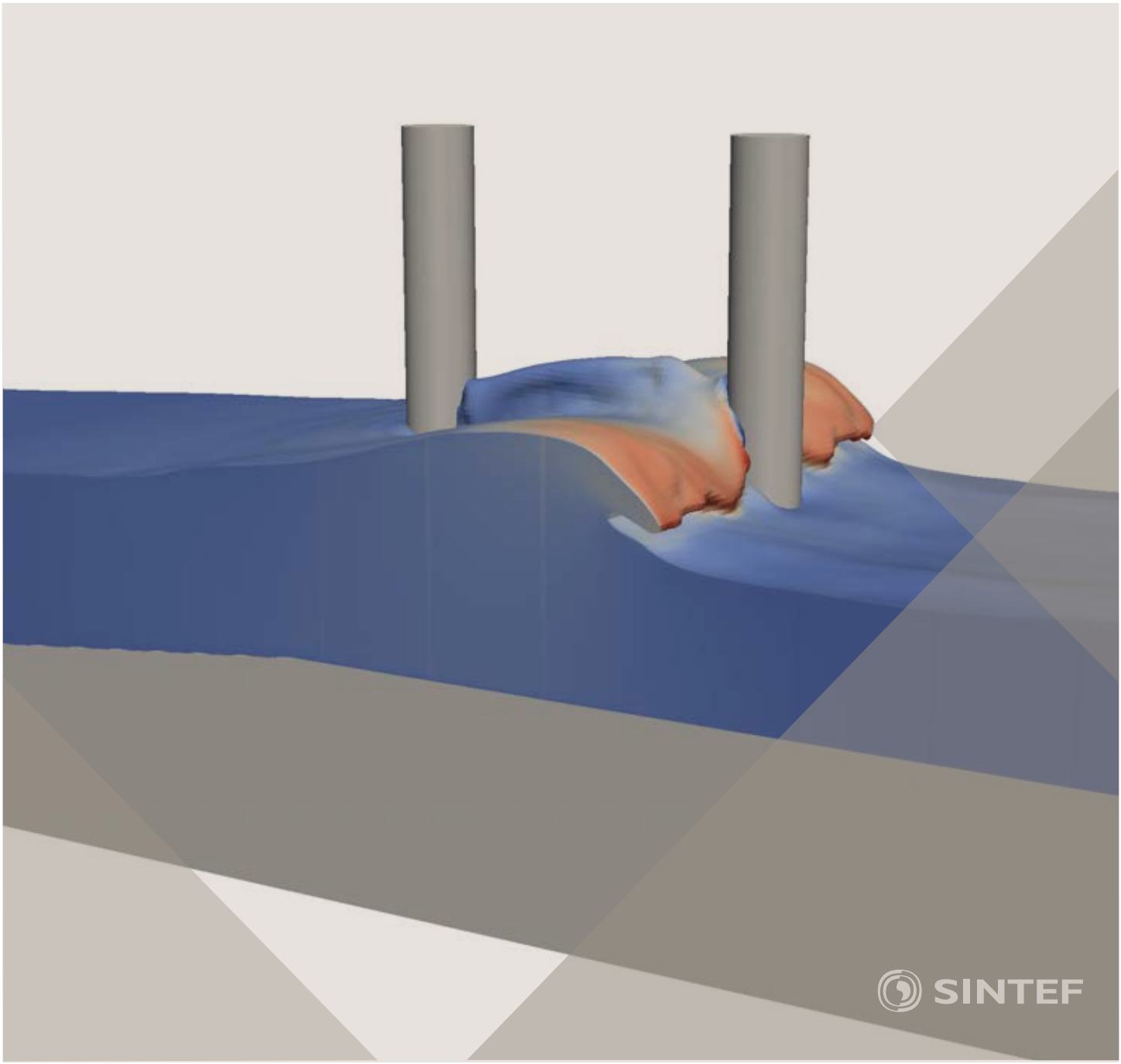

SINTEF Proceedings

Editors:
Jan Erik Olsen and Stein Tore Johansen

Progress in Applied CFD – CFD2017

Proceedings of the 12th International Conference on Computational Fluid Dynamics in the Oil & Gas, Metallurgical and Process Industries

SINTEF Academic Press

SINTEF Proceedings no 2
Editors: Jan Erik Olsen and Stein Tore Johansen
Progress in Applied CFD – CFD2017
Selected papers from 10th International Conference on Computational Fluid Dynamics in the Oil & Gas, Metallurgical and Process Industries

Key words:
CFD, Flow, Modelling

Cover, illustration: Arun Kamath

ISSN 2387-4295 (online)
ISBN 978-82-536-1544-8 (pdf)

SINTEF Academic Press
Address: Forskningsveien 3 B
PO Box 124 Blindern
N-0314 OSLO
Tel: +47 73 59 30 00
Fax: +47 22 96 55 08

www.sintef.no/byggforsk
www.sintefbok.no

SINTEF Proceedings
SINTEF Proceedings is a serial publication for peer-reviewed conference proceedings on a variety of scientific topics.
The processes of peer-reviewing of papers published in SINTEF Proceedings are administered by the conference organizers and proceedings editors. Detailed procedures will vary according to custom and practice in each scientific community.

PREFACE

This book contains all manuscripts approved by the reviewers and the organizing committee of the 12th International Conference on Computational Fluid Dynamics in the Oil & Gas, Metallurgical and Process Industries. The conference was hosted by SINTEF in Trondheim in May/June 2017 and is also known as CFD2017 for short. The conference series was initiated by CSIRO and Phil Schwarz in 1997. So far the conference has been alternating between CSIRO in Melbourne and SINTEF in Trondheim. The conferences focuses on the application of CFD in the oil and gas industries, metal production, mineral processing, power generation, chemicals and other process industries. In addition pragmatic modelling concepts and bio-mechanical applications have become an important part of the conference. The papers in this book demonstrate the current progress in applied CFD.

The conference papers undergo a review process involving two experts. Only papers accepted by the reviewers are included in the proceedings. 108 contributions were presented at the conference together with six keynote presentations. A majority of these contributions are presented by their manuscript in this collection (a few were granted to present without an accompanying manuscript).

The organizing committee would like to thank everyone who has helped with review of manuscripts, all those who helped to promote the conference and all authors who have submitted scientific contributions. We are also grateful for the support from the conference sponsors: ANSYS, SFI Metal Production and NanoSim.

Stein Tore Johansen & Jan Erik Olsen

Organizing committee:

Conference chairman: Prof. Stein Tore Johansen
Conference coordinator: Dr. Jan Erik Olsen
Dr. Bernhard Müller
Dr.Sigrid Karstad Dahl
Dr.Shahriar Amini
Dr.Ernst Meese
Dr.Josip Zoric
Dr.Jannike Solsvik
Dr.Peter Witt

Scientific committee:

Stein Tore Johansen, SINTEF/NTNU
Bernhard Müller, NTNU
Phil Schwarz, CSIRO
Akio Tomiyama, Kobe University
Hans Kuipers, Eindhoven University of Technology
Jinghai Li, Chinese Academy of Science
Markus Braun, Ansys
Simon Lo, CD-adapco
Patrick Segers, Universiteit Gent
Jiyuan Tu, RMIT
Jos Derksen, University of Aberdeen
Dmitry Eskin, Schlumberger-Doll Research
Pär Jönsson, KTH
Stefan Pirker, Johannes Kepler University
Josip Zoric, SINTEF

CONTENTS

MULTIPHASE FLUID FLOW MODELLING OF FURNACE TAPHOLES

Quinn G. REYNOLDS[1*] , Markus W. ERWEE[1]**

[1] MINTEK Pyrometallurgy Division, Randburg, Johannesburg, 2125, SOUTH AFRICA

* E-mail: quinnr@mintek.co.za
** E-mail: markuse@mintek.co.za

ABSTRACT

Pyrometallurgical furnaces of many varieties make use of tapholes in order to facilitate the removal of molten process material from inside the vessel. Correct understanding and operation of the taphole is essential for optimal performance of such furnaces.

The present work makes use of computational fluid dynamics models generated using the OpenFOAM® framework in order to study flow behaviour in the taphole system. Single-phase large-eddy simulation models are used to quantify the discharge rate and laminar-turbulent transitions as a function of parameters such as height of material inside the furnace vessel, taphole geometry, and fluid properties. The results are used to inform boundary conditions in multiphase fluid flow models used for prediction of the qualitative behaviour of the free surface in the launder and tapping ladle for selected cases.

Keywords: CFD, Pyrometallurgy, Tapholes, Furnace.

NOMENCLATURE

Greek Symbols

ρ Mass density, [kg/m^3].
μ Dynamic viscosity, [kg/m.s].

Latin Symbols

D Diameter of taphole, [m].
L Length of taphole [m].
P Pressure, [Pa].
$\mathbf{u}$ Velocity, [m/s].

Dimensionless

N_{Re} Reynolds number.
N_L Geometry ratio.
N_T $N_{Eu}.\sqrt{N_{Re.}}$
N_{Eu} Euler number.
K_L Discharge coefficient.

INTRODUCTION

Many important commodities such as iron and steel, aluminium, ferro-alloys, and precious metals are produced in part using pyrometallurgical furnaces (Jones et al., 2006). The majority of these units make use of tapholes, specially-designed openings in the furnace wall, in order to remove the molten process products from the furnace (Nelson et al., 2016). Depending on the commodity being produced, the furnace may use a single taphole for all material, or separate tapholes for different phases such as slag and metal. Tapholes are typically located in a taphole assembly, a section of the furnace sidewall designed for this purpose. The taphole assembly may consist of several cylindrical or rectangular inserts made of copper, graphite, or refractory material through which the taphole itself runs, mounted within a steel frame which provides structural support and a contact point for water cooling (McDougall, 2014).

Figure 1: Tapping in operation on a DC furnace pilot plant, (l) and (m) slag, (r) metal (images courtesy Mintek)

After the taphole is opened by lancing or drilling, molten material drains out of the vessel due to differences in hydrostatic pressure (see Figure 1). The rate of drainage is primarily determined by a combination of the inlet geometry and the length of the taphole channel, as well as the physical and thermochemical properties of the material passing through the taphole. Characterisation of the flow behaviour inside the taphole channel is challenging due to the wide variation in physical properties of the fluid phases encountered in furnaces; metals and sulphide mattes tend to be high-density and low-viscosity, while oxide slags are the opposite. Transitions between turbulent and laminar flow may occur during a tap or even within the taphole itself, especially for higher-viscosity materials; such transitions affect not only the discharge rate of material through the taphole but also the mechanical forces on the taphole

surfaces which contribute to erosion and wear, and may be exacerbated by gas entrainment during tapping (He et al., 2002).

Upon exiting the taphole, the molten material passes through an open channel (the tapping launder) and into a steel or refractory-lined container vessel (the tapping ladle). The launder and ladle system is a multiphase free surface flow problem, behaviour of the fluid flow is highly dependent on the physical properties of the material being tapped. In practice launders may be angled both vertically and horizontally in order to reach tapping ladles located below, ladles may be positioned incorrectly, and wear on the lining of the launder may change its shape form the original design. As a result, substantial splashing and intermixing of the molten phase with the surrounding air may occur. Although this is undesirable in the case of reduction smelting or high-purity product requirements, the degree of contact between the air and the molten product is generally small and can be further mitigated by careful launder and ladle design and operation (Leong et al., 2006).

To date, much research has been conducted in the field of computational modelling of taphole flow behaviour using advanced modelling techniques (e.g. (Kadkhodabeigi et al., 2011) and (Shao et al., 2013)). However, due to the high resource demands of accurate computational fluid dynamics modelling, there is generally a strong focus on specific design problems or process parameters, using computational fluid dynamics as a post hoc design analysis or failure forensics tool. In the present work, the intention is to use computational modelling as a virtual experimentation platform in order to gain insight into the behaviour of taphole systems at a more generalised and simplified level.

FLOW THROUGH THE TAPHOLE – THEORY AND DIMENSIONAL CONSIDERATIONS

For the taphole region geometry as described in Figure 2, it is instructive to consider initially a simple theoretical expression for the fluid flow into and through the taphole. Similar work has been performed elsewhere (e.g. (Guthrie, 1992) using the Bernoulli equation to relate the imposed pressure differential across the taphole to the flowrate of material through it. This approach results in:

$$\Delta P = \frac{\rho u^2}{2} + P_P + P_E \qquad (1)$$

Where ΔP is the pressure difference between the furnace interior and exterior as a result of static head of molten material and any additional forces, ρ is the fluid density, u is the bulk average velocity of fluid in the taphole, and P_P and P_E are the irreversible pressure losses due to viscous flow inside the taphole channel and friction in the taphole entry geometry respectively. Bulk velocity of the fluid in the furnace interior is assumed to be close to zero.

If fully-developed laminar flow in the taphole channel is assumed, (1) may be written as:

$$\Delta P = \frac{32\mu L u}{D^2} + (1 + K_L)\frac{\rho u^2}{2} \qquad (2)$$

where μ is the fluid viscosity, L and D are the taphole length and diameter respectively, and K_L is the discharge coefficient for a given entry geometry (0.5 for sharp-edged pipe entries, reducing to negligible values for well-rounded inlets resulting from advanced taphole wear). Rearranging (2) in terms of dimensionless quantities yields:

$$N_T^2 = \frac{1 + K_L}{2} N_{Re}^2 + 32 N_L N_{Re} \qquad (3)$$

Here, N_{Re} is the Reynolds number, N_L is a simple geometry ratio, and N_T is the product of the Reynolds number and the square root of the Euler number. By the principles of dimensional analysis only these three groups are needed to completely define the problem regardless of the flow regime; their definitions are shown in Table 1.

Table 1: Dimensionless groups used to characterise taphole flow

N_{Re}	N_L	N_T
$\frac{Du\rho}{\mu}$	$\frac{L}{D}$	$\frac{D\sqrt{\rho\Delta P}}{\mu}$

This particular set of dimensionless groups is preferred since only one (N_{Re}) is dependent on the fluid velocity, which is often a poorly-known quantity in tapping operations. This allows tapping velocity to be represented explicitly as a function of the taphole design, the properties of the fluid being tapped, and the applied pressure.

MODEL DEVELOPMENT

In order to model different aspects of the behaviour of taphole systems most effectively, several simplifications were made.

Although the effect of heat transfer and phase change on the molten material being tapped is an important aspect of the taphole's behaviour, this study focuses only on flow in order to isolate behaviour related to fluid dynamics. Coupled heat transfer models will be considered at a later stage but are not within the scope of the present work.

In addition, the taphole system was divided into two separate computational models – one covering the single-phase flow from the furnace interior to the exit point of the taphole, and another covering the multiphase flow from the taphole exit through the launder and into the ladle. The rationale for this approach as opposed to a single unified model is that different research questions are posed in the different regions – in flow through the taphole, it is desirable to perform high fidelity

simulations in order to resolve near-wall turbulence and accurately quantify the discharge rate as a function of taphole geometry and fluid properties, whereas with flow in the launder and ladle the primary aim is to identify broad qualitative differences in the patterns of free surface flow in response to variations in material properties and equipment design.

Both computational models were implemented using the finite volume method, in OpenFOAM® version 4.1 (OpenFOAM, 2017). For the taphole region model, a modified version of the "pisoFoam" solver was written to allow for adaptive time-stepping using a specified Courant number. For the launder and ladle region model, the standard "interFoam" solver was used without modification. Hexahedral-element-dominant computational meshes were generated using cfMesh version 1.1.1 (cfMesh, 2017), with mesh sizes ranging from between 1 and 2 million elements for the taphole region models, up to ~4 million elements for the launder and ladle region models.

Taphole region model

Flow in the taphole region is modelled using large eddy simulation (LES) methods to capture the turbulent flow behaviour. LES methods directly compute the unsteady, dynamic behaviour in turbulent flow at length scales above a certain level, and approximate the turbulent stresses using sub-grid scale (SGS) models at length scales below it. The critical length scale is commonly taken as the resolution of the numerical mesh. This approach results in a filtered version of the Navier Stokes equations for the resolved components of the pressure and fluid velocity, containing source terms which are closed using the chosen SGS model. LES models generally require higher-fidelity meshes than Reynolds-averaged (RANS) turbulence models, but are considerably less computationally demanding than direct numerical simulation. They are more adept than RANS models with regard to predicting laminar-turbulent transition behaviour as well as temporal structures in turbulent flows, both of which are relevant to the present study.

For the taphole region a dynamic k-equation model (Kim et al., 1995) is used as the SGS model together with standard box filtering at the mesh resolution. Near-wall mesh refinement was used to ensure that the dimensionless wall distance y^+ remained below unity.

The entry region and taphole channel are modelled as a large plenum zone (representing the furnace interior) connected to a cylindrical pipe section (representing the taphole itself). The lip of the taphole is treated as a sharp edge, and assumes that little or no wear of the taphole materials of construction has occurred. The geometry of the model region is shown in Figure 2.

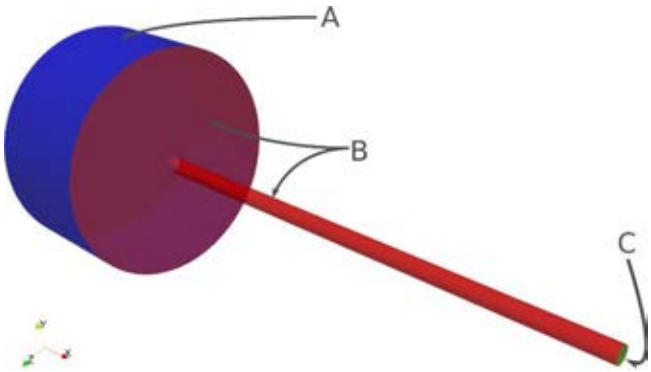

Figure 2: Taphole model geometry

Boundary conditions are applied as shown in Table 2.

Table 2: Boundary conditions for taphole region model

Boundary	**u**	p	k
A (inlet)	$\frac{\partial u_n}{\partial \mathbf{n}} = 0$ $u_\tau = 0$	$p = \frac{\Delta P}{\rho} - \frac{1}{2}\lvert\mathbf{u}\rvert^2$	$k = 0$
B (walls)	$\mathbf{u} = 0$	$\frac{\partial p}{\partial \mathbf{n}} = 0$	$k = 0$
C (outlet)	$\frac{\partial \mathbf{u}}{\partial \mathbf{n}} = 0$	$p = 0$	$\frac{\partial k}{\partial \mathbf{n}} = 0$

In the case of the reduced pressure boundary condition on boundary A, the boundary value of p is calculated using the total applied pressure difference across the domain (a specified parameter, as used in equations (1) to (3)) and the local velocity at the boundary, which is obtained after calculation of the velocity field boundary condition.

Here, **u** is the fluid velocity vector field (with components u_n and u_τ normal and tangential to the boundary respectively), p is the reduced pressure field, k is the turbulent kinetic energy field, and **n** are unit vectors normal to the boundary surface.

Launder and ladle region model

In the region after the molten material exits the taphole, the behaviour is modelled using the volume of fluid (VOF) method for multiphase fluid flow (Hirt et al., 1981). VOF tracks the fluid interface using a phase field α, representing the volume fraction of the first phase (in a two-phase system, the volume fraction of the second phase is then $1 - \alpha$). The evolution of α is modelled with a convection equation using gradient compression schemes to maintain a sharp interface between phases. Source terms are added to the Navier Stokes equations in the interface regions to account for the additional forces arising from surface tension effects.

The launder and ladle are modelled as solid walls surrounded by open atmosphere as shown in Figure 3. The ladle is treated as a simple truncated conical vessel in all cases, but the launder is modelled with different designs (rectangular and v-shaped channel profiles) to examine the effect on the flow patterns while tapping. Slag and metal materials are modelled in each case to

examine the effect of the physical properties of the molten phase on the behaviour of the system. A range of taphole exit velocities is considered based on results obtained from the taphole region model. Static mesh refinement is performed in each case by running an initial simulation at low resolution, and using the resulting phase field to refine the mesh to higher resolution in areas where the gas-liquid interface is present. Boundary conditions used are shown in Table 3.

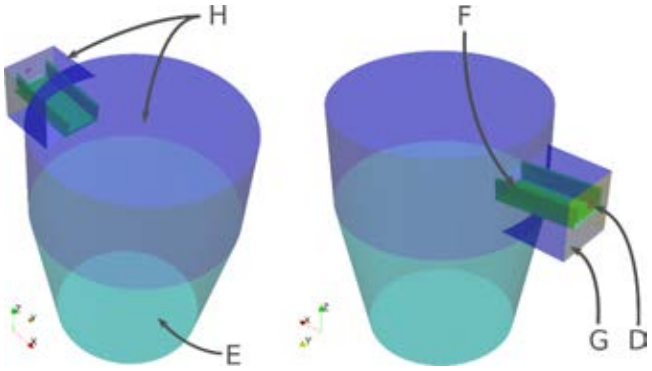

Figure 3: Geometry of launder and ladle models

Table 3: Boundary conditions for ladle and launder region model

Boundary	**u**	P	α
D (inlet)	$\mathbf{u} = \mathbf{u}_0$	$\frac{\partial P}{\partial \mathbf{n}} = 0$	$\alpha = 1$
E, F, G (walls)	$\mathbf{u} = 0$	$\frac{\partial P}{\partial \mathbf{n}} = 0$	$\frac{\partial \alpha}{\partial \mathbf{n}} = 0$
H (atmosphere)	$\begin{cases} \frac{\partial u_n}{\partial \mathbf{n}} = 0, \ u_\tau = 0 \\ \frac{\partial \mathbf{u}}{\partial \mathbf{n}} = 0 \end{cases}$	$\begin{cases} P = P_0 - \frac{1}{2}\rho\lvert\mathbf{u}\rvert^2 \\ P = P_0 \end{cases}$	$\begin{cases} \alpha = 0 \\ \frac{\partial \alpha}{\partial \mathbf{n}} = 0 \end{cases}$

In the case of the absolute pressure boundary condition on boundary H, the boundary value of P is calculated using the specified total atmospheric pressure and the local velocity at the boundary, which is obtained after calculation of the velocity field boundary condition.

Here, P is the absolute pressure field, and P_0 is atmospheric pressure in the region around the launder and ladle. α represents the volume fraction of molten material. At the atmosphere boundary F, it is possible for fluid to flow both into and out of the domain – for each field, the first expression is used in the case of inflow, the second in the case of outflow.

Model parameters

The viscosities, densities and surface tension values of slags, mattes and metals vary with both composition and temperature. These properties are often difficult to measure, due to the extreme temperatures at which these phases are molten. A detailed summary of the viscosity and density values for various commodity smelting operations in given in (Nelson et al., 2016). For iron and steel production, ferroalloys such as ferrochromium and ferromanganese, the viscosity of the metal phase at temperature varies between 0.004 and 0.007 Pa.s. For mattes (e.g. from copper and nickel smelting operations), the values can be higher – varying from 0.003 to 0.05 Pa.s The viscosity of slags from these operations varies between 0.1 to 1.5 Pa.s across operations, except for copper smelting where the slag viscosity values are as low as 0.03 Pa.s. Notably, the viscosity of slags in any operation can increase dramatically when solids precipitate from the melt.

Density values vary from 5500 to 7500 kg/m³ for ferrous-based processes, typically 4200-4500 kg/m³ for mattes. Slag density values vary between 2600-3200 kg/m³ for most slags, except for, for example copper and nickel process slags, which generally slightly higher densities, roughly 3500 – 4000 kg/m³.

The surface tension values for metals and slags in pyrometallurgical processes are quite high (when compared to common fluids). These values vary across commodities, but is roughly 0.5 N/m for most common slags, mattes and metals (Tanaka et al., 2014).

In terms of the physical design and operation parameters of the taphole region, typical lengths and diameters for slag, metal, and matte tapholes have been reported in several sources, for example (Nelson et al., 2016), (van Beek et al., 2014), and (Nolet, 2014). A summary of the industrial data is shown in Table 4. Although the internal furnace pressure in the case of certain processes such as blast furnaces can be extremely high (up to 5 bar (Nelson et al., 2016)), in open-bath smelting furnaces the primary source of the pressure is most often the head of molten material above the level of the taphole. Typical values across several different processes are reported in (Nelson et al., 2016) and summarised in Table 5.

Table 4: Geometry parameters for industrial furnace tapholes

Material	Taphole diameter	Taphole length
Slag	0.04 – 0.1 m	< 1.3 m
Matte	0.04 – 0.1 m	1 – 1.5 m
Metal	0.04 – 0.07 m	1 – 1.5 m

Table 5: Head of molten material above tapholes for slag and metal/matte systems

Material	Above slag taphole	Above metal/matte taphole
Slag	0.2 – 1 m	0.4 – 2 m
Metal/matte	-	0.15 – 0.6 m

In order to demonstrate the use of the multiphase flow model of the launder and ladle region, dimensions based on pilot-scale DC furnace equipment in use at Mintek were selected. Two different launder cross sections, a square channel profile and a v-shaped channel profile, were studied at different flowrates of slag and metal material to determine their impact on the flow pattern into the ladle. Dimensions of the model system are shown in Table 6.

Table 6: Geometry parameters for launder and ladle models

Parameter	Value	Parameter	Value
Taphole diameter	0.03 m	Ladle diameter	1 m
Launder length	0.4 m	Ladle height	0.75 m
Launder width	0.2 m	Launder height above ladle	0.2 m
Launder inclination	5°		

RESULTS AND DISCUSSION

Taphole region models

In order to study a broad range of typical taphole conditions and designs representative of most electric smelting processes, a set of simulations was executed to cover the ranges $500 < N_T < 500000$, and $10 < N_L < 50$. This was achieved in the computational model by fixing taphole diameter (0.02 m), fluid density (7000 kg/m^3), and applied pressure (89286 Pa), and calculating the required taphole length and fluid viscosity in each case based on the desired values of N_T and N_L using the expressions in Table 1.

Once the initial conditions had decayed sufficiently (typically after 1 s of simulation time), a time- and area-averaged velocity at the taphole outlet was computed and used to calculate N_{Re}. The laminar or turbulent nature of the flow was assessed using the relative variability in time of the velocity field at the outlet – this was calculated by finding the difference between the minimum and maximum velocity values at the taphole centreline over the final 0.2 s of simulation time divided by the average outlet velocity over the same time period. A total of 32 separate cases were simulated using the sharp-edged entry geometry shown in Figure 2, each taking between 10 and 20 hours of wall time on 16 Intel Xeon CPUs.

For model validation purposes, the simulation results were compared to the predictions of equation (3) in the laminar flow region. This is shown in Figure 4. The agreement in both qualitative trends and values is fairly good, with the computational model under-predicting slightly relative to (3). This is expected since (3) assumes that the flow in the taphole is fully developed along its entire length, whereas in reality there will be an entrance length over which the wall boundary layer expands before full Hagen-Poisiuelle flow is reached. In this entry region, the wall shear forces are higher and will therefore restrict the flow to a greater degree, resulting in lower flowrates than those predicted by (3).

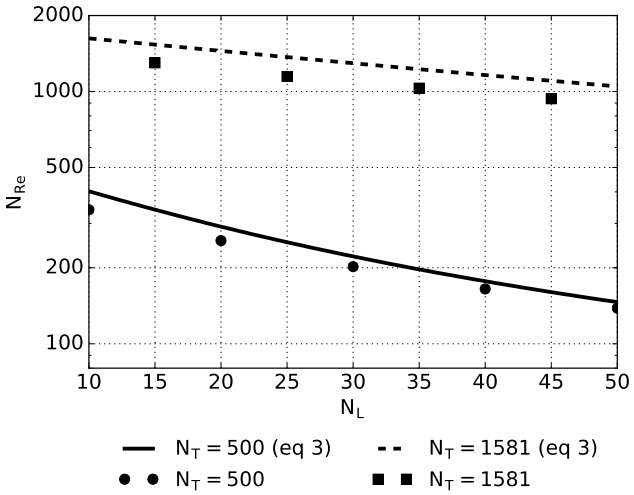

Figure 4: Model validation against equation (3)

Visualisations of the instantaneous flow patterns in and around the taphole are presented in Figures 5 to 7, for cases in which the value of N_L was fixed at 30 and the value of N_T was changed. All visualisations are shown at the end of the simulation, time = 1 s. The upper section of each image shows the velocity profile through the 3D volume, and the lower section shows a contour plot of turbulent viscosity ν_t.

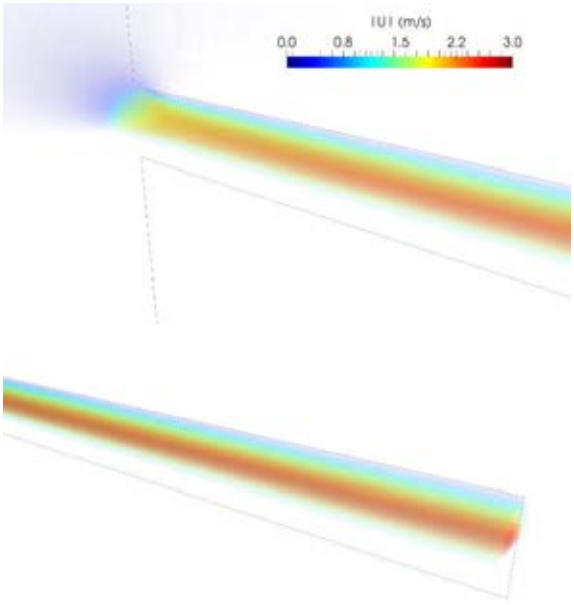

Figure 5: Velocity field (coloured) and contour of ν_t = 7.5 x 10^{-6} m^2/s for case N_L = 30 and N_T = 500, (top) taphole entry (bottom) taphole exit

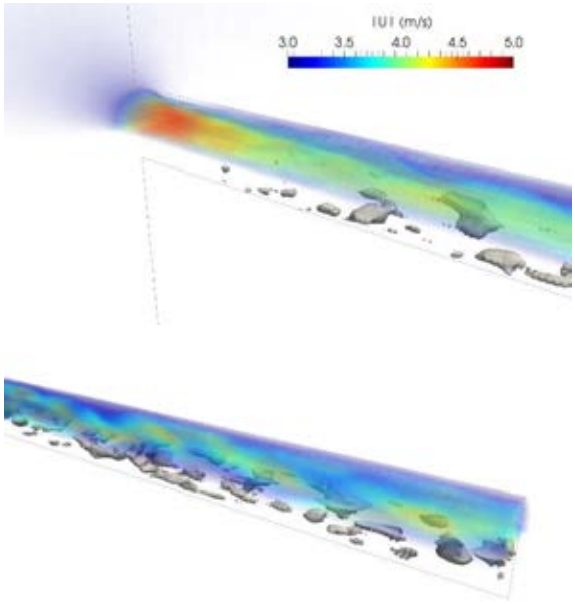

Figure 6: Velocity field (coloured) and contour of ν_t = 7.5 x 10^{-6} m^2/s for case N_L = 30 and N_T = 5000, (top) taphole entry (bottom) taphole exit

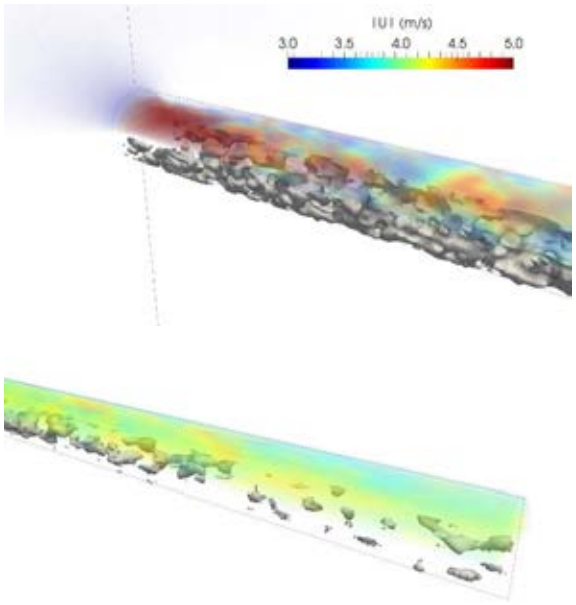

Figure 7: Velocity field (coloured) and contour of ν_t = 7.5 x 10^{-6} m^2/s for case N_L = 30 and N_T = 500000, (top) taphole entry (bottom) taphole exit

As N_T increases, a transition from laminar to unsteady, turbulent flow occurs. In particular, a vena contracta with flow separation forms in the entry region of the taphole due to the sharp-edged entry, and this acts as a strong trigger for turbulent flow to develop in this area at high N_T. Average flow velocity increases steadily from approximately 1.5 m/s at N_T = 500 to 4 m/s at N_T = 500000. Detail of the evolution of the velocity field along the centreline of the taphole over time is shown in Figure 8 and 9 for cases of laminar and turbulent flow (in both cases, x/L = 0.2 indicates the location of the taphole entry). It may be seen that the turbulent flow case exhibits erratic and unsteady flow starting within one or two diameters of the taphole inlet at approximately 0.1 s, and propagating down the taphole channel at the bulk average flow velocity.

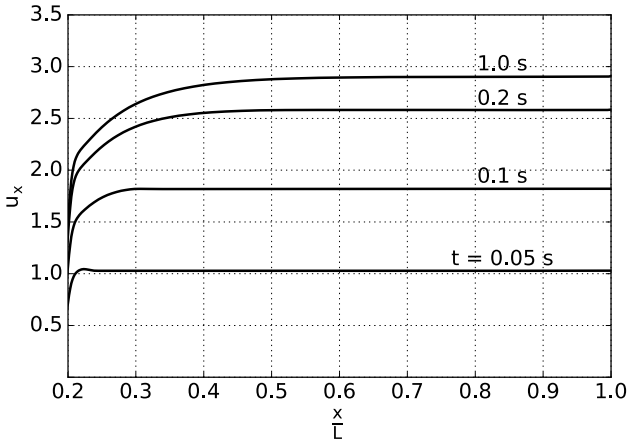

Figure 8: Evolution of instantaneous velocity profile along taphole centreline as a function of time, case N_L = 30 and N_T = 500 (laminar flow)

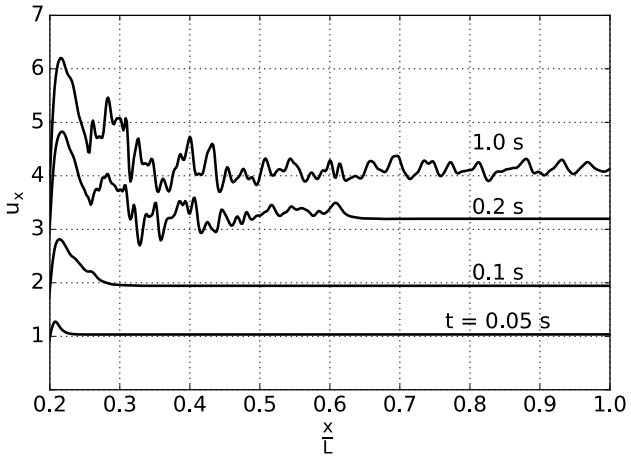

Figure 9: Evolution of instantaneous velocity profile along taphole centreline as a function of time, case N_L = 30 and N_T = 500000 (turbulent flow)

Changing the length of the taphole while holding N_T constant results in less extreme changes in the behaviour of the flow, however certain differences are visible. Visualisation of the flow patterns for short and long tapholes are presented in Figures 10 and 11. In the case of tapholes with early turbulent triggering as is the case with sharp-edged entry geometry, the level of turbulence at the taphole exit is generally seen to be higher for shorter tapholes (this is somewhat exacerbated by the fact that shorter tapholes result in higher discharge velocities, although this is a second-order effect). Turbulence levels settle within 10 to 15 taphole diameters and remain constant in longer tapholes. This suggests that mechanical wear patterns may be expected to be more uniform in longer tapholes away from the entry region.

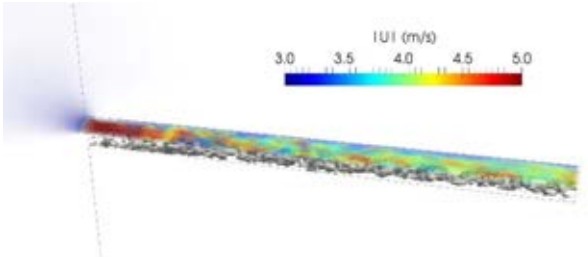

Figure 10: Velocity field (coloured) and contour of ν_t = 7.5 x 10^{-6} m^2/s for case N_L = 15 and N_T = 15811

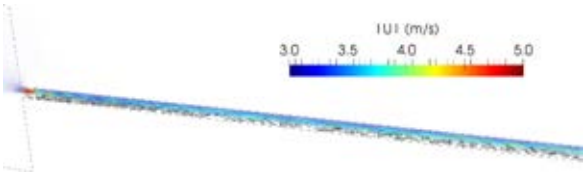

Figure 11: Velocity field (coloured) and contour of ν_t = 7.5 x 10^{-6} m^2/s for case N_L = 45 and N_T = 15811

The full set of computational model results for the prediction of N_{Re} as a function of N_L and N_T was linearly interpolated and is presented in Figure 12. It can be seen that increasing the taphole length has a significant effect on the discharge velocity only at relatively low values of N_T, below about 10^4. Dependence of N_{Re} on N_T is strong in all operating regions, increasing approximately linearly as N_T and N_L become large – this is expected since N_T is proportional to the square root of the applied pressure, which is the driving force for the flow. It is also interesting to note that since N_{Re} and N_T are both proportional to D/μ, the viscosity and taphole diameter have a relatively small effect on the discharge velocity in this range; it is instead dominated by the density of the molten material and the applied pressure at the taphole entrance.

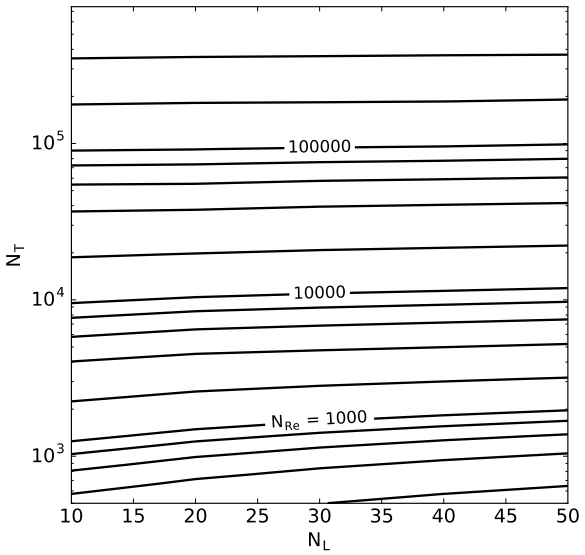

Figure 12: N_{Re} calculated by computational model as a function of N_L and N_T

In Figure 13, the transition from laminar to turbulent flow as calculated from the model results using the variability of the velocity at the taphole outlet is presented. The transition region is assumed to be a function of N_{Re} for a given taphole geometry – the bounds were estimated using the lowest value of calculated N_{Re} for which the model predicted unsteady flow, and the highest value of N_{Re} for which steady laminar flow was predicted. When indicative operating regions for slag, matte, and metal tapholes are imposed on the chart, it can be seen that metals and mattes are in general very likely to exhibit turbulent flow in at least part of the taphole, whereas slags may be laminar or turbulent (or even transition from one to the other during a single tap) depending on the conditions. This has implications for the wear mechanisms occurring at the taphole channel surface; in general, turbulent flow may be expected to exacerbate mechanical wear of the taphole.

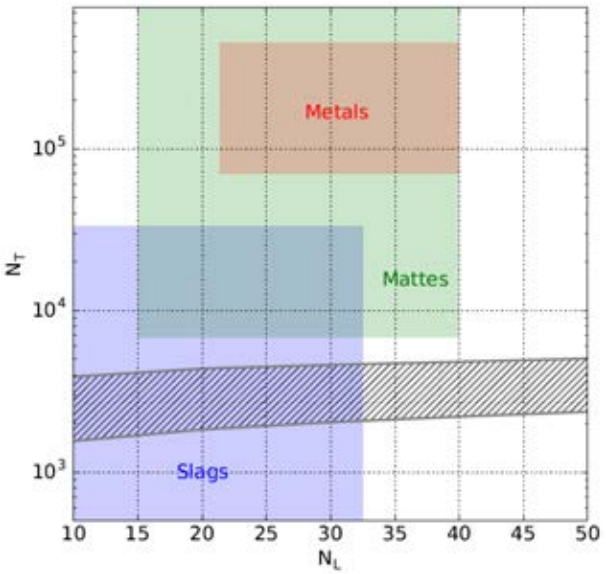

Figure 13: Laminar-turbulent transition region (grey hatching) showing typical operating windows for slag, metal, and matte tapholes

Although results for sharp-edged entries are useful for predicting flow through new tapholes, it is also of interest to consider how the flow patterns change once the taphole has worn after repeated use. Taphole wear patterns are typically concentrated in the entry region, resulting in conical (Thomson, 2014) or rounded (Steenkamp et al., 2014) inlets. Computational models of worn tapholes were constructed assuming an increase in the channel radius at the entry point of 0.05 m, and wear into the channel to a depth of 0.05 m. Visualisations of the flow patterns from models at N_L = 30 and N_T = 50000 are shown in Figures 14 and 15. When compared to results from the sharp-edged taphole models, it can be seen that the smoother the entrance geometry relative to the local direction of flow, the lower the level of turbulence generated in the taphole entrance region. This is particularly obvious in the case of the rounded entrance, in which the onset of turbulent flow is postponed an appreciable distance down the taphole channel even at high values of N_T. This observation suggests that the pattern of mechanical wear in furnace tapholes may change as the taphole ages – wear is initially concentrated in the entrance region, but reduces and moves into the main body of the taphole as time goes on.

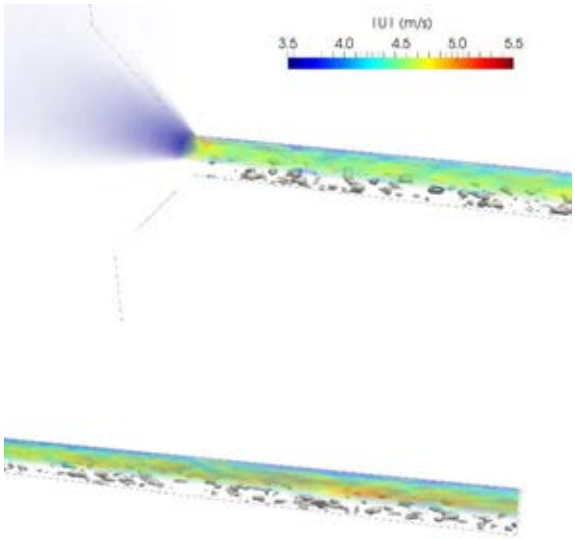

Figure 14: Velocity field (coloured) and contour of ν_t = 7.5 x 10^{-6} m^2/s for case N_L = 30 and N_T = 50000 with conical entrance, (top) taphole entry (bottom) taphole exit

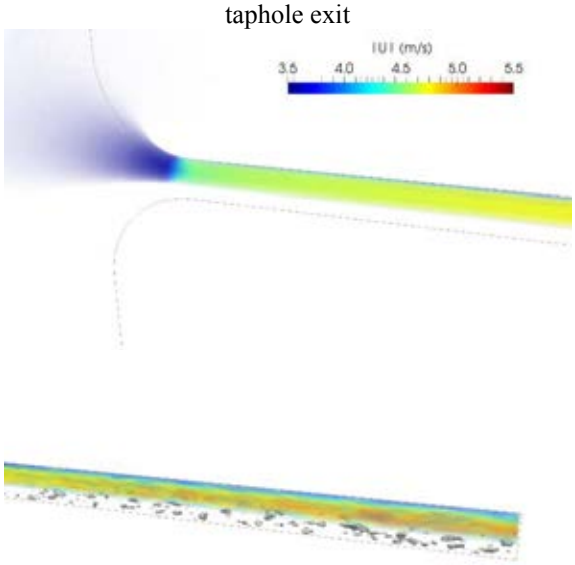

Figure 15: Velocity field (coloured) and contour of ν_t = 7.5 x 10^{-6} m^2/s for case N_L = 30 and N_T = 50000 with rounded entrance, (bottom) taphole entry (top) taphole exit

Although there are considerable qualitative differences in the flow patterns and turbulence onset, the quantitative differences in flow velocity are relatively small for different entry configurations. Figure 16 shows a comparison of the sharp-edged entry results with those from conical and rounded entry models.

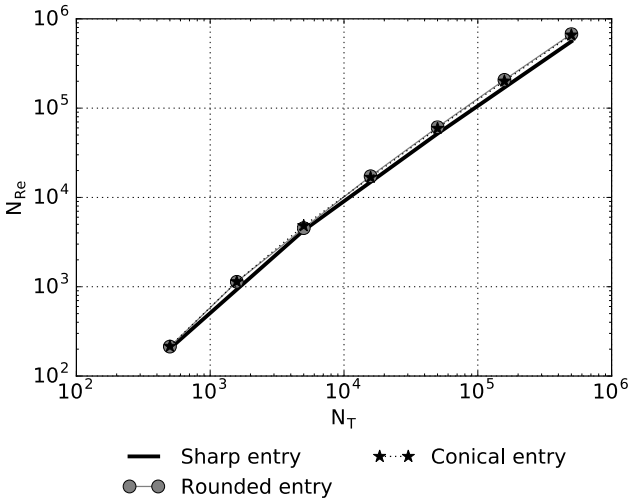

Figure 16: N_{Re} calculated by computational model as a function of N_T at N_L = 30, for different entry geometries

It can be seen that the tapping velocities match within 10-20 % across a wide range of N_T for all geometries tested, although more comprehensive study is recommended to verify this result.

Ladle and launder region models

The results from the taphole region model determine appropriate ranges on the taphole exit velocity, which is required as an input boundary condition for the launder and ladle region model – in the case of a pilot-scale furnace as modelled here, exit velocities between 1 and 3 m/s were applied. For the liquid phase being tapped, both slag (μ = 0.1 Pa.s, ρ = 2500 kg/m^3) and metal (μ = 0.005 Pa.s, ρ = 7000 kg/m^3) materials were used. For the surrounding gas phase, the properties of air were used.

Results comparing different materials and flowrates for the rectangular launder design are shown in Figures 17 to 20, in all cases at time 4 s after taphole opening. The contour of α = 0.1 is used to show the liquid surface, and coloured according to the local velocity field.

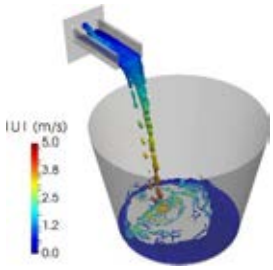

Figure 17: Rectangular profile launder, slag tapping at 1 m/s

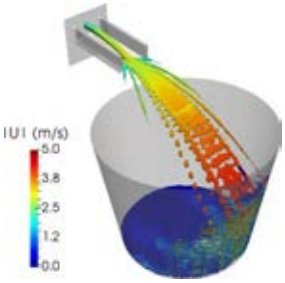

Figure 18: Rectangular profile launder, slag tapping at 3 m/s

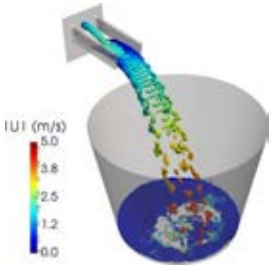

Figure 21: Rectangular launder profile, slag tapping at 2 m/s

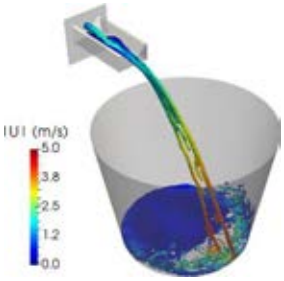

Figure 22: V-shaped launder profile, slag tapping at 2 m/s

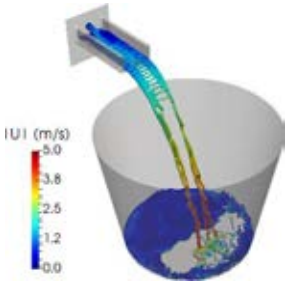

Figure 19: Rectangular launder profile, metal tapping at 1 m/s

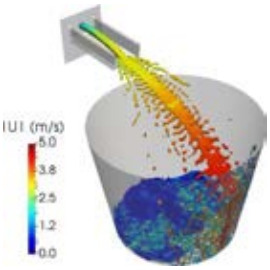

Figure 20: Rectangular launder profile, metal tapping at 3 m/s

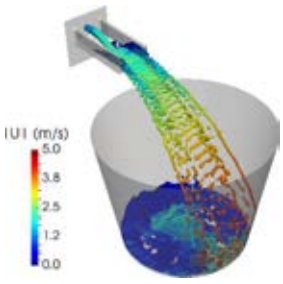

Figure 23: Rectangular launder profile, metal tapping at 2 m/s

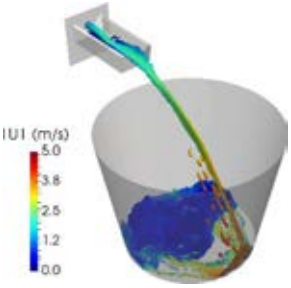

Figure 24: V-shaped launder profile, metal tapping at 2 m/s

At low flowrates, the tapping stream is generally well contained within the launder channel with minimal splashing before exiting into the ladle. At high flowrates (typical of when the taphole is newly opened) it is clear that this particular launder design is too short – the tapping stream catches the edge of the launder and spreads the tapped material out into a fan shape as it enters the ladle. This would not be an optimal configuration for tapping metal, as the increased surface area may result in undesirable re-oxidation of the material by the surrounding air as it enters the ladle.

Comparing different materials, it can be seen that in the case of metal the flow tends to separate out into smaller droplets and streams than in the case of slag; it is likely that this is related to the lower viscosity of molten metals. The flow patterns at low tapping velocities are particularly different, due to the development of open-channel flow patterns in the launder in addition to the free-surface flow as the material exits into the ladle.

Results comparing a simple variation on the launder design are shown in Figures 21 to 24. Flow behaviour at a fixed tapping velocity (2 m/s) is shown in all cases, with visualisations performed at 4 s after the taphole was opened. The contour of $\alpha = 0.1$ is used to show the liquid surface, and coloured according to the local velocity field.

Changing the cross-sectional shape of the launder has a significant impact on the shape and structure of the flow regardless of the material being tapped. In the case of the v-shaped launder, the channel flow is kept contained in a narrower cross-section as it traverses the launder, resulting in a more contained stream flowing into the ladle. This results in less break-up of the stream into droplets, keeping the surface area exposed to air lower. The intense, directed flow of the stream into the ladle may however cause high localised heat transfer and mechanical wear of the ladle lining – this would have to be managed carefully to avoid premature ladle failure.

CONCLUSIONS

Characterisation of the flow behaviour in furnace taphole systems is a complex subject. Due to the practical challenges associated with handling of molten materials at high temperatures, computational modelling can be used very effectively as a complement to experimental work in this area. Development of preliminary computational models of the fluid flow behaviour both inside the taphole and after the material exits it have been successful, and study of a range of operating parameters and designs was conducted.

The taphole region models demonstrated that for typical material properties and taphole geometries, the nature of the flow inside the taphole can be expected to be turbulent for metals and mattes, but may be laminar or turbulent for slags depending on conditions. Quantification of the taphole exit velocities in terms of dimensionless parameters was obtained, with dependence of N_{Re} on N_T being much stronger than on N_L. The effect of taphole entrance geometry on turbulence onset and flow patterns in the taphole channel was found to be appreciable, however, the exit velocities were not particularly sensitive to this change.

The results from the taphole region model were used as boundary conditions for multiphase flow models of the launder and ladle outside the furnace. The scope of this work was limited to comparing the flow behaviour in a simple design at pilot-plant furnace scale. It was found that differences in flow patterns between slag and metal were exaggerated at low tapping velocities, with metal flows tending to break up into smaller droplets and streams. Launder channel shape also had a large effect on the nature of the free surface flow between the launder and the ladle, suggesting that proper launder design and maintenance is critical for repeatable tapping flow behaviour.

This work is intended to be a preliminary starting point for computational modelling of taphole flow behaviour, and as such, there is considerable scope for further research in this area. In the taphole region, more detailed studies of fluid dynamics in the taphole channel using LES or direct numerical simulation models which include the effect of taphole wear on geometry and surface roughness would be of value. In the launder and ladle region, evolution of the model into a virtual prototype capable of comparative performance testing of various designs is anticipated. In all cases the impact of coupling additional phenomena (in particular heat transfer and phase change) to the flow model should be investigated further, and ultimately integrated into the thermal design of the taphole assembly.

ACKNOWLEDGEMENTS

This paper is published by permission of Mintek. The CSIR Centre for High Performance Computing provided computational resources for execution of all modelling work. The authors gratefully acknowledge useful interactions with Lloyd Nelson and Rodney Hundermark (Anglo American plc), and Joalet Steenkamp (Mintek).

REFERENCES

JONES, R.T. and CURR, T.R. (2006). “Pyrometallurgy at Mintek”, *Proc. SAIMM Southern African Pyrometallurgy 2006*, Johannesburg, South Africa, p 127.

NELSON, L.R. and HUNDERMARK, R.J. (2016). “’The tap-hole’ – key to furnace performance”, *J. SAIMM*, 116(5), p 465.

MCDOUGALL, I. (2014). “Water cooled tap-hole blocks”, *Proc. SAIMM Furnace Tapping Conference 2014*, Muldersdrift, South Africa, p 183.

HE, Q., ZULLI, P., TANZIL, F., LEE, B., DUNNING, J., and EVANS, G. (2002). “Flow characteristics of a blast furnace taphole stream and its effects on trough refractory wear”, *ISIJ*, 42(3), p 235.

LEONG, B. and JOUBERT, H. (2006). “Innovative and safe copper launder design”, *Proc. SAIMM Southern African Pyrometallurgy 2006*, Johannesburg, South Africa, p 385.

KADKHODABEIGI, M., TVEIT, H., and JOHANSEN, S.T. (2011). “Modelling the tapping process in submerged arc furnaces used in high silicon alloys production”, *ISIJ*, 51(2), p 193.

SHAO, L. and SAXEN, H. (2013). “A simulation study of two-liquid flow in the taphole of the blast furnace”, *ISIJ*, 53(6), p 988.

GUTHRIE, R.I.L. (1992). “Engineering in process metallurgy”, Oxford University Press, Oxford, United Kingdom.

OpenFOAM (2017). https://www.openfoam.org/, accessed 10/02/2017.

cfMesh (2017). http://cfmesh.com/, accessed 10/02/2017.

KIM, W.-W. and MENON, S. (1995). “A new dynamic one-equation subgrid-scale model for large eddy simulations”, *Proc. AIAA 33rd Aerospace Sciences Meeting and Exhibit*, Reno NV, USA, paper 1995-0356.

HIRT, C.W. and NICHOLS, B.D. (1981). "Volume of fluid (VOF) method for the dynamics of free boundaries", *J. Comput. Phys.*, 39(1), p 201.

TANAKA, T. and SCHELLER, P.R. “Interfacial Phenomena in High Temperature Metallurgy”, *Chapter 1 in Treatise on Process Metallurgy Volume 2: Process Phenomena*, edited by Seetharaman, S., McLean, A., Guthrie, R. and Sridhar, S., Elsevier, 2014, pp.46-50.

VAN BEEK, W.S.B., GOFF, T.J., NEL, P.E., and REX, E. (2014). “An overview of the design, operation, and maintenance practices relating to tap-hole management of a PGM smelting furnace”, *Proc. SAIMM Furnace Tapping Conference 2014*, Muldersdrift, South Africa, p 113.

NOLET, I. (2014). “Tapping of PGM-Ni mattes: an industry survey”, *Proc. SAIMM Furnace Tapping Conference 2014*, Muldersdrift, South Africa, p 223.

THOMSON, L. (2014). “Monitoring, repair, and safety practices for electric furnace matte tapping”, *Proc. SAIMM Furnace Tapping Conference 2014*, Muldersdrift, South Africa, p 87.

STEENKAMP, J.D, GOUS, J.P., PISTORIUS, P.C., TANGSTAD, M., and ZIETSMAN, J.H. (2014). “Wear analysis of a tap-hole from a SiMn production furnace”, *Proc. SAIMM Furnace Tapping Conference 2014*, Muldersdrift, South Africa, p 51.